

# Practical Considerations for Full Duplex Enabled 5G Integrated Access and Backhaul

Sergey Shaboyan<sup>1</sup> · Alireza S. Behbahani<sup>1</sup> · Ahmed M. Eltawil<sup>1</sup>

Received: 29 July 2019 / Revised: 19 September 2019 / Accepted: 15 November 2019 / Published online: 21 January 2020 © Springer Science+Business Media, LLC, part of Springer Nature 2020

#### **Abstract**

With the advent of 5G networks means for backhauling network traffic emerged as a major consideration. Densification via small cell deployment has made wired solution cost prohibitive, leading to the adoption of spectrally efficient wireless solutions, namely, Integrated Access and Backhaul (IAB). This paper discusses the different options for IAB and focuses on novel solutions for in-band IAB using Full Duplex (FD) enabled nodes. Dynamically reconfigured beam steering antennas are presented as a means of passively suppressing Self-Interference (SI). Experimental results confirm up to 65 dB of SI cancellation in a harsh environment with obstacle. Finally, robust methods for managing FD practical considerations including timing and frequency offsets are presented, with experimental results confirming performance.

**Keywords** Integrated access and backhaul · Full duplex · 5G · Small cells

## 1 Introduction

Demand for wireless network capacity keeps growing exponentially every year. As a result, a large increase in data traffic is projected over the next 10 years in the context of 5G wireless networks. In order to boost network capacity and expand coverage, the concept of deploying low-cost, low-power small cells (SCs) over traditional macro cell networks has been investigated [1–4]. Dense SC deployment brings users closer to the base stations resulting in improved wireless connectivity. With multiple-antenna arrays at the SCs, hybrid beamforming can be leveraged to achieve higher transmission gains, reduce the transmitting power, and mitigate interference between co-tier users [5]. While RF solution below 6 GHz offer the best Non-Line-of-Sight (NLoS) performance and coverage, spectrum below 6

GHz is congested. Millimeter-wave spectrum (frequencies over 24 GHz) offers wider, multi-GHz channel bandwidths, and therefore has gained significant research interest as a promising solution to address data traffic demands of 5G. Massive deployment of small cells will be a key feature of the emerging 5G cellular networks [6], requiring efficient forwarding of backhaul traffic.

By definition, small cell backhaul connections are used to

- 1. Forward/receive the end-user (small cell user) data to/from the core network.
- 2. Exchange mutual information among different small cells.

The backhaul evolution for 5G small cells will include wired (e.g., optical fiber) and wireless backhauling (e.g., microwave or millimeter wave links) to and from core network aggregators (e.g., macro base stations (MBSs)), and cooperation through anchor base stations (A-BSs), etc.). Since the backhaul requirements can significantly vary depending on the locations of small cells, the cost of implementing backhaul connections, traffic load intensity of small cells, latency, and target quality of service requirement, there is no single optimal approach for the backhauling of small cells.

While wired backhaul solutions ensure reliability with high data rates, the cost of wired connections is highly dependent on the offered capacity as well as the distance,

Sergey Shaboyan sshaboya@uci.edu

Alireza S. Behbahani sshahanb@uci.edu

University of California, Irvine, 4412 Engineering Hall, Irvine, CA, 92697, USA



Ahmed M. Eltawil aeltawil@uci.edu

and can become rapidly prohibitive. Wireless backhauling is rapidly becoming adopted as a viable and cost-effective approach that allows operators to obtain end-to-end control of their network rather than leasing third party wired backhaul connections. Key wireless backhaul solutions leverage exploiting the sub-6 GHz band, satellite technologies, microwave spectrum between 6 GHz and 60 GHz bands, and millimeter wave (mmWave) spectrum in 60 GHz and 70 to 80 GHz bands. An optimal selection of the wireless backhaul solution depends on the propagation environment as well as a number of system parameters such as locations and deployment density of small cells, desired backhaul capacity, interference conditions, cost, coverage, hardware requirements, and spectrum availability.

# 1.1 Integrated Access and Backhaul

An interesting use case for SCs in the context of 5G is Integrated Access and Backhaul (IAB). In an IAB setting a node can perform both access to a user as well as backhaul as shown in Fig. 1 and described in the 3GPP study on integrated access and backhaul which recognizes IAB as a viable and cost effective means of enabling dense 5G networks [7–9]. The document investigates architectures, radio protocols, and physical layer aspects for sharing radio resources between access and backhaul links and defines IAB as follows: "In-band backhauling includes scenarios where access- and backhaul link at least partially overlap in frequency creating half-duplexing or interference constraints, which imply that the IAB-node cannot transmit and receive simultaneously on both links. In the present context, out-of-band scenarios are understood as not posing such constraints.

While the study presents solutions for both in-band and out-of-band IAB systems, it focuses on partial or full in-band solutions due to the anticipated spectral efficiency associated with in-band systems. IAB nodes are expected to operate in either a stand alone (SA) mode where the node is connected to the 5G network or in a non-stand alone (NSA) where it is connected to 4G Evolved Packet Core

(EPC). Topologies under consideration include a Directed Acyclic Graph (DAG) where IAB-nodes connect to multiple up-stream nodes, or spanning tree where each IAB node is connected to one parent. In both topologies, the IAB node is assumed to serve either a User Equipment (UE), or connect to other IAB nodes as a parent or a child node. IAB-donor nodes are nodes that have fiber connectivity for back-hauling and can serve both UEs or other IAB nodes.

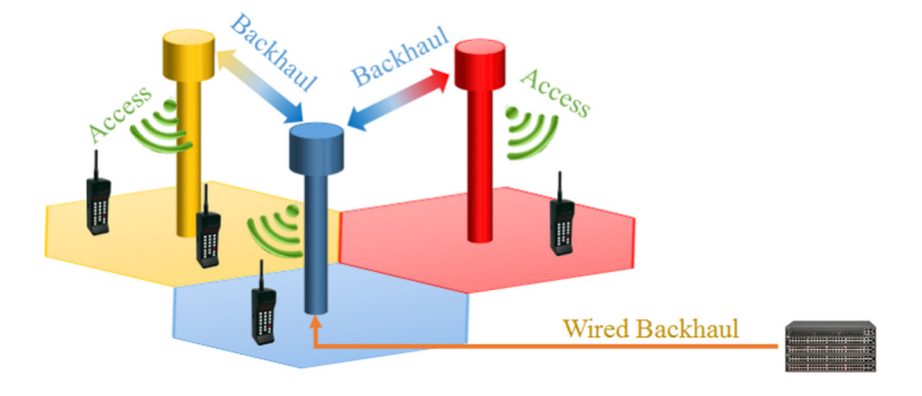
Each IAB node can have two radio functions, either as a Mobile Termination (MT), or a Distributed Unit (DU). MTs are used to maintain the wireless backhaul connection to up-stream IAB-nodes or IAB-donor, while DUs are used to provide access connection to the UEs or the down-stream MTs of other IAB-nodes.

## 1.1.1 Full Duplex IAB

While using traditional half-duplex (HD) radios for SC IAB is the easiest solution and is supported by current radios, it results in poor spectral efficiency or introduces unwanted latency in the network depending on whether Frequency division Duplexing (FDD) or Time Division Duplexing (TDD) is used. This reality becomes painfully limiting in spectrum starved deployment scenarios that operate in sub-6 GHz bands. One solution that has the potential to alleviate these issues is In-Band-Full-Duplex (IBFD) approaches to SC networks. FD systems offer the potential to double capacity and lower latency in which inband FD-enabled SCs relay data from a macro base station (BS) to user equipment (UE) in the same frequency band [10, 11] simultaneously, using self-interference cancellation algorithms [12]. As a result, FD enables ultra-dense SC deployments [13–15], with simple frequency planning since frequency pairing for up-link and down-link is no longer needed. Instead of using a wired backhaul the SCs are connected to the core network via a macro BS over a wireless backhaul, thereby reducing the deployment cost as compared to traditional cellular networks [16].

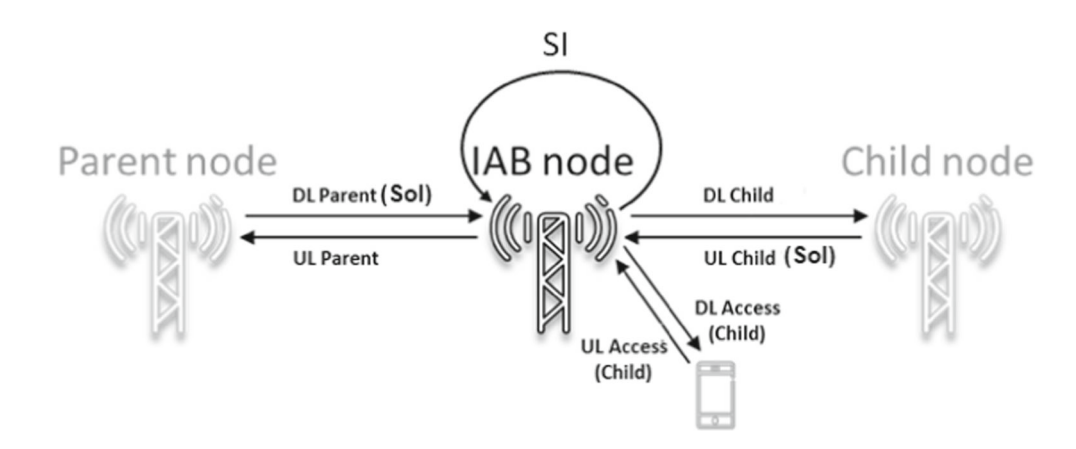
FD can be theoretically deployed at any frequency across the microwave band. For example, deployment of

Figure 1 Integrated Access and backhaul.





**Figure 2** IAB full duplex system.



FD solutions at mm-wave is possible and will benefit from the directivity associated with mm-wave systems. However, mm-wave currently benefits from less congestion as compared to sub 6-GHz band. Thus in this paper we focus on the sub 6-GHz bands where the issue of spectrum congestion is the most obvious, hence increasing the value of FD deployment.

The paper is organized as follows: Section 2 presents an overview of Full Duplex systems in the context of IAB, Self Interference issues are presented and solutions are discussed, a novel reconfigurable beam steering antenna is presented to be used as a means of passive suppression. Section 3 presents experimental results on passive suppression performance and introduces practical FD loop recovery considerations for timing and frequency offsets. Section 4 presents experimental results integrating both passive suppression and timing recovery loops. The paper is concluded in Section 5.

# **2 Full Duplex Systems**

While FD offers numerous advantages, it also comes with a set of challenges. The main challenge in FD systems is managing the self-interference (SI) signal at each node, which is typically orders of magnitude larger than the intended Signal of Interest (SOI). In the context of IAB, the SC can be considered as a relay between the base station and the user equipment. Typically, relays can be classified as either Amplify and Forward (AF) type or

Decode and Forward (DF) type [17]. AFR does not have a demodulation/decoding block in the receive chain, however, it is assumed to have the ability to construct and transmit certain control/management packets as defined by the standard. In contrast, DFR does have ability of decoding and modulating the received data before re-transmission. The signal that the full duplex relay (FDR) is aiming to receive is the signal of interest (SOI). The transmitted signal is also received by its own receiver, causing self-interference as shown in Fig. 2.

Figure 3 focuses on one side of an FDR transaction where a base station (node 1) is communication with a remote node (node 2) in FD fashion. The signal being received from the remote node is refered to as the Signal of Interest (SOI), while the self interference signal is refered to as the SI.

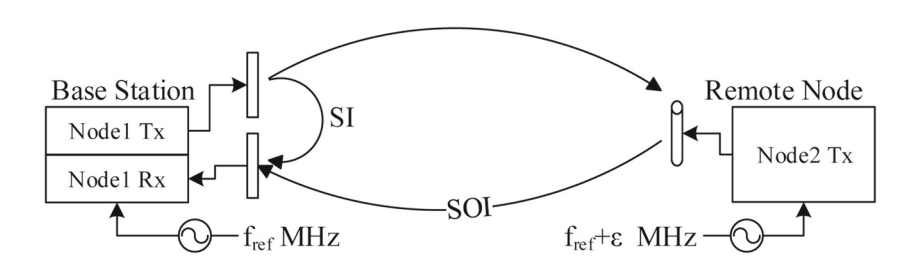
The aggregate received signal by the FDR in the time domain can be modeled as

$$r(t) = s^{tx}(t) * h_{soi}(t) + y^{tx}(t) * h_{si}(t) + w(t)$$
 (1)

where  $s^{tx}(t)$  and  $y^{tx}(t)$  are SOI and SI components of the received signal. w(t) is Additive White Gaussian Noise (AWGN).

From Eq. 1 it is clear that SI must be suppressed in order to achieve satisfactory SINR for the received signal. Numerous techniques are available for SI suppression including passive (eg. antenna separation, directional antennas etc.) and active (analog and digital cancellation). In analog cancellation, subtraction of the self generated SI

**Figure 3** Block diagram of full duplex system.





signal is typically performed before the low noise amplifier, using multi-tap RF filters that mimic the SI wireless channel. If a single antenna is used, RF circulators can be used to provide isolation. In the digital domain, remaining self interference is removed by estimating the SI channel. Other sources of noise such as phase noise and non-linearity are typically addressed by using a single Phase Locked Loop (PLL) to drive both transmit (Tx) and receive (Rx) chains, improving the linearity of both Tx and Rx chains, and using non-linearity estimation loops [18, 19].

In addition to SI suppression, other factors should be considered as well. For example, the increased interference caused by FD and the traffic profile may further compromise theoretical FD gain. FD doubles the amount of interfering streams, leading to an increased inter-cell interference (ICI). Furthermore, exploiting FD is only possible when there is data traffic in both link directions, uplink (UL) and downlink (DL). Another consideration is power consumption, which is a critical challenge in applying FD relaying, because additional power is triggered by self-interference cancellation at the FD relay. Moreover, the receive and transmit chains of FD relaying systems are active at all time, while only one transmit chain or one receive chain of HD relaying is active at each time slot.

# 2.1 SI Suppression

As discussed earlier, SI suppression is key for successful FD deployment. In prior work, we proposed the use of Multi re-configurable antennas (MRAs) to provide up to 70 dB of passive suppression in the propagation domain [19]. An MRA is a single antenna element that can perform multiple functions by dynamically changing its properties. To change the properties of an MRA, the current distribution over the volume of the antenna needs to be changed, where each distribution corresponds to a different mode of operation. To this end, one can change the geometry of the antenna under software control by switching on and off various geometrical segments that make up the MRA using low loss switches. Figure 4 presents an example of a 2.4 GHz MRA (including 3D and 2D radiation patterns associated with a

sample mode) that can provide up to 4096 possible modes of operation by configuring the surface geometry of the parasitic layer. In this particular antenna, the reconfigurable parasitic surface consists of  $3 \times 3$  square-shaped metallic pixels connected by 12 PIN diode switches with ON/OFF status, formed on the top surface of the parasitic layer with individual pixel size being  $15 \times 15 \ mm^2$ . With a digital control word of 12 bits, 4096 modes can be exercised.

## 2.1.1 Passive Suppression Performance

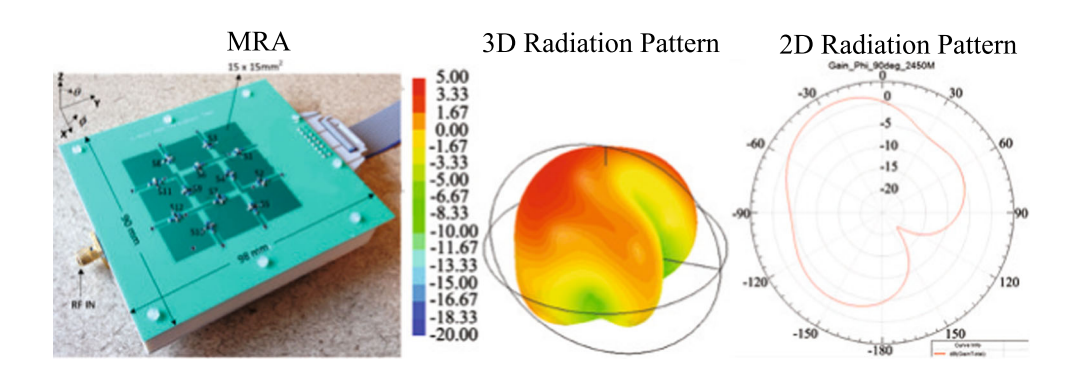
The MRA described earlier was integrated in a complete FD system with two FD nodes. Each node is equipped with one transmit antenna and one receive antenna. In this setup, a omni-directional dipole antenna is used as a transmit antenna, while a 2.4 GHz band multi reconfigurable antenna (MRA) is used as a receiving antenna. Both transmit and receive antennas have the same antenna polarization. The antennas are separated by 10 cm. Pattern selection is performed through a 12-line digital control cable driven from an FPGA on a Zedboard [20]. A pattern selection heuristic that minimizes SI and maximizes the SOI by running a brute search over all possible modes is computed on an attached PC and run in real time on the FPGA of the Zedboard.

The complete FD system is constructed using the Universal Software Radio Peripheral (USRP) software defined radio (SDR) platform streaming samples at 25Msample/sec to a processing PC [20]. All experiments are performed in the 2.4-2.5 GHz ISM band with a 5/10 MHz signal bandwidth. The timing of all USRPs and the FPGA that drives the antenna switches are aligned with one reference Pulse Per Second (PPS) signal. All experimental testing was conducted in the Wireless Systems and Circuits Laboratory (WSCL) within Engineering Hall at the University of California, Irvine. A full description of the experimental setup for the FD platform is available in [19].

# 2.1.2 Experimental Results on SI Suppression

In order to test the performance of passive MRA based SI cancellation, an experiment was setup with electromagnetic

**Figure 4** Reconfigurable Antenna.





reflectors placed between the two nodes. The system was tested using a 1  $m^2$  rectangular foil obstacle (RCS  $\sim$  $100m^2$ ) placed at various distances directly in the line of sight between the communicating nodes as shown in Fig. 5a. The obstacle was moved towards the antenna staring at 5m away and gradually approaching the node as shown in Fig. 5b. A search over all 4096 modes was performed and the winning pattern index displayed for each distance as shown in the figure. Note that for each distance a different pattern is selected. Figure 5c shows that the self-interference signal is well suppressed by choosing the appropriate antenna pattern. Note that even at only 0.5 m away, performance is still maintained at 65 dB cancellation (Tx power is +5 dBm). Finally, Fig. 5d shows the received power from the far node which starts off at around -52 dBm without an obstacle and decreases (as expected) when the obstacle is moved closer to the receiving node. Note that in all cases a winning pattern can be found and that self-interference cancellation was maintained.

# **3 FD System Performance**

In this section we measure the impact of practical consideration such as timing and frequency offsets on overall system performance. We created a model that captures two important practical features of FD systems, namely, a) MRA based SI channel features, and b) FD system timing, including carrier frequency offset and sampling time offset. Finally, we quantify the timing recovery loop performance in the presence of SI residual signal. The characterization performed is performed in the context of Orthogonal Frequency Division Multiplexing (OFDM), where OFDM is the most widely deployed modulation of choice for 5G systems. Each node modulates its data on  $N_{FFT}$  subcarriers that are spaced  $\Delta f$  apart. For sampling frequency  $f_s$ , subcarrier spacing is computed as

$$\Delta f = \frac{f_s}{N_{FFT}} = \frac{1}{N_{FFT}T_s} = \frac{1}{T_{sym}} \tag{2}$$

where  $T_s$  is sampling period and  $T_{sym}$  is one OFDM symbol duration. As a result  $i^{th}$  OFDM block  $z_i$  is expressed as

$$z_{i}(n) = \begin{cases} \frac{1}{N_{FFT}} \sum_{k=0}^{N_{FFT}-1} d_{i}(k) e^{\frac{j2\pi kn}{N_{FFT}}} & 0 \le n < N_{FFT} \\ 0 & otherwise \end{cases}$$
(3)

Cyclic prefix (CP) with time duration of  $N_{CP}$  is appended before each OFDM symbol, which serves as guard interval

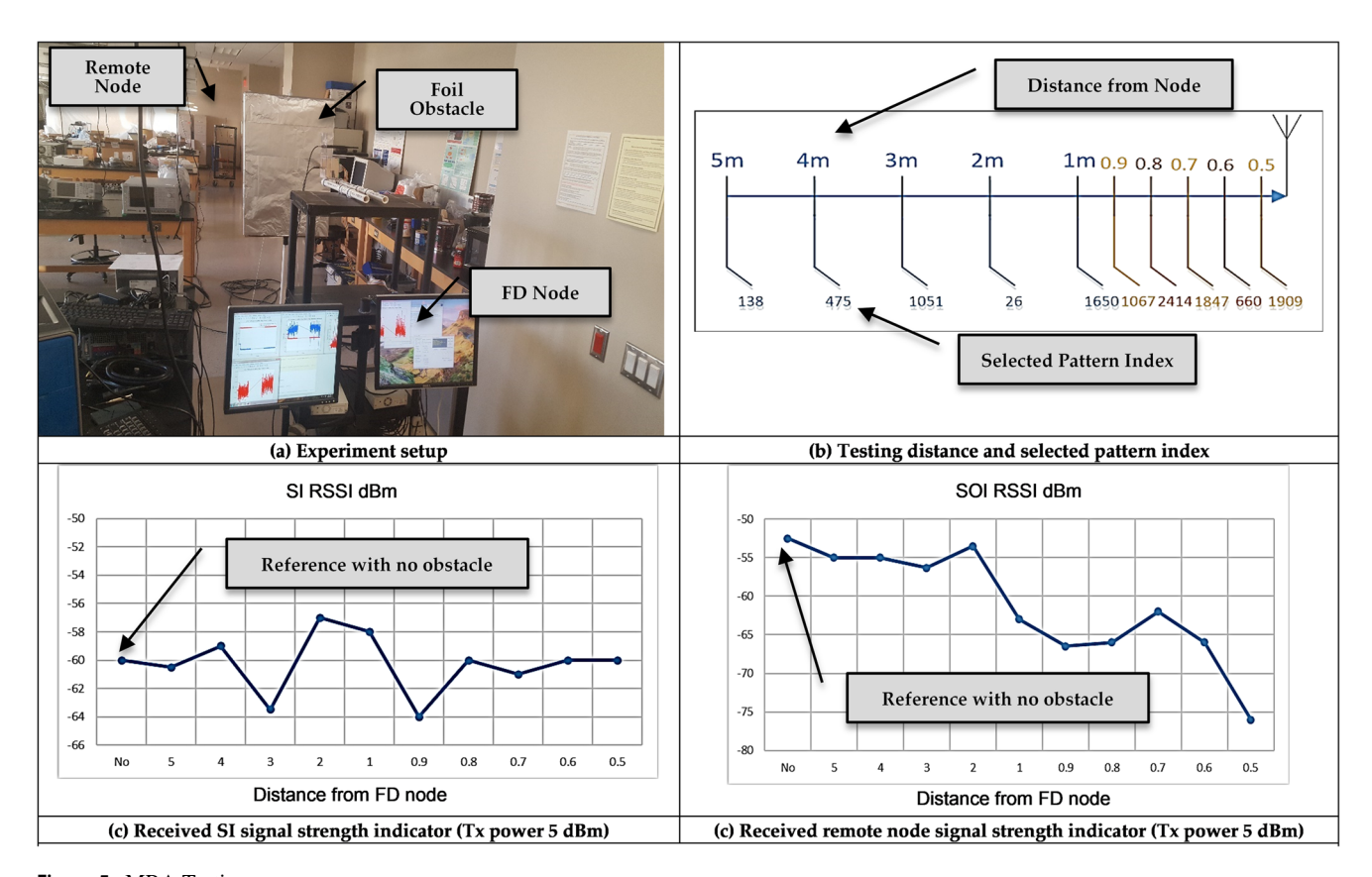
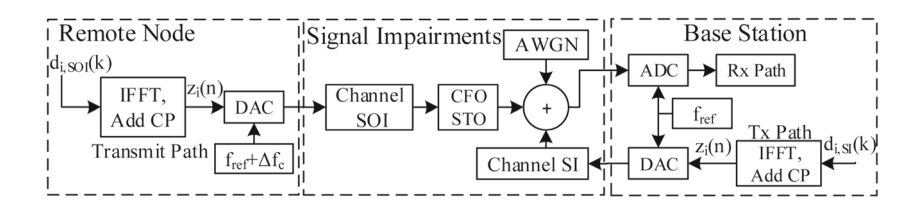


Figure 5 MRA Testing.



**Figure 6** Full-Duplex Channel Model.



between two adjacent blocks and helps avoiding intersymbol interference (ISI). Finally each digital block is transformed into analog signal, up-converted to the carrier frequency  $f_c$  and transmitted over the wireless channel.

Figure 6 illustrates a typical OFDM based structure for a FD enabled system representing both SOI and SI propagation [21]. SOI channel,  $h_{soi}$ , is modeled to reflect path loss and Rayleigh fading effects. SOI is impacted by carrier frequency offset (CFO) and sampling time offset (STO) due to the local oscillator (LO) mismatch  $\Delta f_c$ . CFO can be modeled as a constant positive or negative frequency shift. STO is modeled as fractional delay filter, which applies time-varying lead or lag.

The SI channel,  $h_{si}$ , is modeled to reflect path loss and Rayleigh fading effects. In addition, it assumes the use of passive self interference suppression using the MRA system described earlier. The SI signal does not experience either CFO or STO because both the transmitter and receiver are co-located at the base station and share the same clock frequency. Finally, AWGN is added to the composite signal containing a superposition of the two signals.

## 3.1 FD System Timing Imperfections

Figure 6 illustrates a typical OFDM based structure for a FD enabled system representing both SOI and SI propagation.

At the receiver, the signal is down-converted to baseband and sampled using an Analog to Digital Converter (ADC) (Fig. 6). Due to the fact that the remote node uses a separate, asynchronous clock from that of the transmitter, a mismatch in the remote node transmitter's local oscillator ( $LO_{TX}$ ) and receiver's local oscillator ( $LO_{RX}$ ) frequency and phase is

inevitable and will also be slowly time variant. Thus, their generated frequencies will be off by  $\Delta f_c$  resulting in CFO. The DAC at the remote node transmitter and the ADC at the receiver are also driven by  $LO_{TX}$  and  $LO_{RX}$  respectively, thus, after digitization, the received signal samples will experience STO. Therefore, the received  $i^{th}$  block of data  $u_i$  can be expressed as follows:

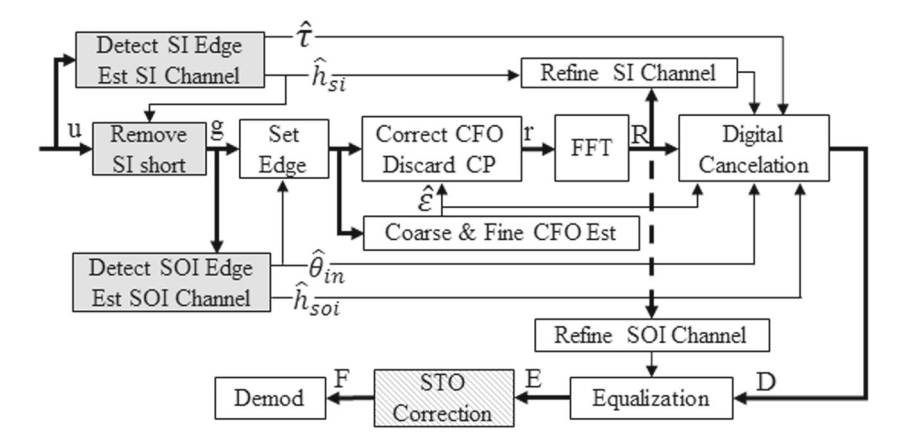
$$u_{i}(n) = e^{\frac{j2\pi \varepsilon n}{N_{FFT}}} s_{i}^{tx}(n-\theta) * h_{soi}(n) + y_{i}^{tx}(n-\tau) * h_{si}(n) + w(n)$$
(4)

where  $s^{tx}(t)$  and  $y^{tx}(t)$  are SOI and SI components of the transmitted signal.  $\varepsilon$  is the relative carrier frequency error, defined as  $\varepsilon = \Delta f_c/\Delta f$ ,  $\theta$  represents time shift of SOI due to STO, and  $\tau$  represents time shift of SI due to channel delay. Time offset  $\theta$  is a gradually increasing quantity which can have integer, as well as, fraction parts  $\theta = \theta_{in} + \theta_{fr}$ . Offset  $\tau$  is relatively constant and can be treated as integer quantity.

As compared to half-duplex, in full-duplex communication, the received signal represents the superposition of two signals transmitted by two different transmitters as shown in Eq. 4. Directly applying a correction to the composite signal, will always lead to having one signal component corrected, while corrupting the other. i.e. if the SOI component is compensated for in the composite signal, the SI component will be corrupted, since operations performed on the received signal will affect both signal components. For proper demodulation, the receiver must recover the transmitted signal  $s_i^{tx}(n)$  from  $u_i(n)$ .

Figure 7 illustrates the block diagram of an OFDM receiver supporting IBFD synchronization. The shaded

**Figure 7** OFDM receiver diagram with IBFD synchronization.





blocks in the figure indicate processing steps that are novel to this architecture as opposed to a standard OFDM receiver. Frame edge detection is performed based on the modified frame structure presented in [20]. The digital cancellation block is modified to account for the estimated timing and frequency offsets. A key difference in this architecture is that STO is performed after digital cancellation rather than at the beginning of the receive chain. The reason this approach is needed in FD systems is to avoid SI corruption when performing SOI CFO/STO correction. Comparing FD receiver architecture with typical HD receiver presented in [22], it is obvious that the complexity of FD receiver is higher. In FD mode, the receiver has to detect two block boundaries, estimate two channels and perform digital cancellation. Therefore synchronization complexity of FD receiver is approximately doubled, comparing to HD counterpart. In the following section we present an overview of the building blocks, while highlighting the sequence of operations necessary for recovering the transmitted signal  $s_i^{tx}(n)$ . Detailed descriptions of each block are presented in subsequent sections.

## 3.1.1 Receiver Signal Processing Flow

First, the receiver estimates initial SI time offset  $\tau$  and uses it to cancel the short training part of SI from received signal  $u_i(n)$ . Then it estimates the integer part of the SOI sampling offset  $\theta_{in}$  and frequency offset  $\varepsilon$  from  $g_i(n)$ . The estimated time offset is removed from the received signal  $g_i(n)$  for proper Fast Fourier Transform (FFT) window placement over SOI, followed by SOI complex phase rotation compensation as shown below

$$r_i(n) = g_i(n + \hat{\theta}_{in}) \cdot e^{-\frac{j2\pi\hat{\epsilon}n}{N_{FFT}}}$$
(5)

where  $\hat{\theta}_{in}$  is the estimated integer part of sampling offset  $\theta$  and  $\hat{\varepsilon}$  is estimated frequency offset. Once SOI is free of CFO and FFT window is aligned with its  $i^{th}$  block, the CP is discarded and the FFT is computed. The output of the FFT is vector R with length  $N_{FFT}$  and can be expressed as

$$R(k) = S_{\theta_{fr}}^{tx}(k)H_{soi}(k) + Y_{\tau-\hat{\theta}_{in}}^{tx}(k+\hat{\varepsilon})H_{si}(k) + W(k)$$
 (6)

where  $S^{tx}(k)$  and  $Y^{tx}(k)$  are frequency domain representations of  $s^{tx}(n)$  and  $y^{tx}(n)$  respectively, subscript  $\tau - \hat{\theta}_{in}$  indicates shift in time domain in positive direction.  $H_{soi}(k)$  and  $H_{si}(k)$  are frequency domain representations of  $h_{soi}(k)$  and  $h_{si}(k)$  respectively.

To perform digital cancellation, the receiver must construct the interferer as accurately as possible to match the interferer term given in Eq. 6. For this reason, the digital canceler utilizes the knowledge of the estimated initial SI time offset  $\hat{\tau}$ , estimated integer sampling offset  $\hat{\theta}_{in}$ ,

estimated frequency offset  $\hat{\varepsilon}$ , and Lest Square (LS) estimate of SI channel  $\hat{H}_{si}(k)$ . Therefore, vector at the output of digital canceler is denoted D, and can be expressed as

$$D(k) = S_{\theta_{fr}}^{tx}(k)H_{soi}(k) + Y_{\tau-\theta_{in}}^{tx}(k+\hat{\varepsilon})H_{si}(k) - Y_{\tau-\theta_{in}}^{tx}(k+\hat{\varepsilon})\hat{H}_{si}(k) + W(k)$$
 (7)

$$D(k) = S_{\theta_{fr}}^{tx}(k)H_{soi}(k) + W_{si}(k) + W(k)$$
 (8)

where  $W_{si}(k)$  is the residual uncompensated self-interference, and is due to SI channel estimation error [21].

To remove the channel effect  $H_{soi}$  impacting  $S^{tx}(k)$ , the receiver performs equalization by estimating the channel  $\hat{H}_{soi}(k)$  of SOI using LS estimation and compensating for it. The vector at the output of equalizer is denoted E can be expressed as

$$E(k) = S_{\theta fr}^{tx}(k) \frac{H_{soi}(k)}{\hat{H}_{soi}(k)} + W_{si}(k) + W(k)$$

$$E(k) = S_{\theta f_r}^{tx}(k) + W_{soi}(k) + W_{si}(k) + W(k)$$
(9)

where  $W_{soi}(k)$  is the residual uncompensated channel effect on the  $S^{tx}(k)$  signal, that appears as an additional noise term, and is due to SOI channel estimation error.

At this point the signal of interest is still impacted with fractional sampling time offset  $\theta_{fr}$ , which has a gradually increasing nature due to the time drift. In general, channel equalization compensates for fractional timing offset, however for long OFDM frames, symbols located farther away from the training, gain additional fractional offset and undergo degradation in SINR.

To compensate for the fractional timing offset, receiver estimates additional channel change  $\hat{H}_{ep}(k)$  on a per symbol basis, and compensates for it. Output of the timing offset correction block can be expressed as

$$F(k) = S^{tx}(k) + W_{ep}(k) + W_{soi}(k) + W_{si}(k) + W(k)$$
 (10)

where  $W_{ep}(k)$  is an additional noise term per-symbol channel estimation error. At this point, F(k) consists of only  $SOI^{tx}(k)$  plus noise terms. As a last step, F(k) is forwarded to the demodulator for data extraction.

# 4 Simulation and Experimental Results

The full-duplex system shown in Fig. 3 is investigated by simulation and experimentally, where the Base Station is equipped with passive and digital SI suppression stages. All simulations and experiments are performed according to the parameters listed in Table 1.



**Table 1** Simulation parameters

OFDM parameters	Value
Number of OFDM Subcarriers	64
Number of Data Subcarriers	44
Number of Pilots	4
Cyclic Prefix (CP)	$3.2\mu s$
Tx Power	5dBm
Rx SI Power	-65 dBm
Sampling Rate	5 MHz

## 4.1 Simulation

The full duplex system is simulated using channel model in Fig. 6. Packets belonging to SOI are impacted with frequency and timing offset. Packets belonging to SI have passive suppression of 70dB due to the use of directional antennas as described earlier. Based on the simulation parameters, the theoretical SINR bound is computed to be equal to 26dB. SINRs of theoretical, perfectly synchronized, synchronization error compensated and synchronization error uncompensated systems are presented in Fig. 8. From the figure, it is clear to see that the SINRs of theoretical, perfectly synchronized, synchronization error compensated are very close to each other up to 70 ppm and vastly improved as compared to an uncompensated system. Figure 9 illustrates the difference in SINR between the ideally synchronized and compensated systems as compared to theory. The ideally synchronized assumes perfect knowledge of the timing and frequency offset parameters at the receiver while the compensated system estimates these variables. At zero offset, both systems show a fixed offset from theory which grows gradually for the compensated system. However, even at 70 ppm, only 0.7dB of degradation is recorded.

# 4.2 Experimental Setup for Timing

The experimental system described earlier was used to test the system timing. As shown in Fig. 3, Node 1 is equipped with one transmit and one receive antenna. Node 2 uses only one antenna. A dipole omni-directional antenna is used as transmit antenna, while a reconfigurable directional antenna is used as a receive antenna. Both transmit and receive antennas have the same antenna polarization. The reconfigurable antenna has a total of 4096 different possible radiation patterns. A successful pattern, is a pattern that maximizes the SOI signal and minimizes the SI signal. The reference clock is generated locally at each node. A sinewave generator, Agilent N9310, is used to generate the reference clock at node 2. This enables control over the reference clock frequency, to test system performance at different frequency offset amounts. Due to measurement equipment reference clock offset tolerance limitation, the maximum offset possible is 25ppm.

## 4.2.1 Experimental Results

The full-duplex system described above was tested in a fully synchronized (by-wire synchronized), compensated and uncompensated modes, and performance was recorded. For each offset value, transmission of over 250 OFDM frames is performed. Each ppm value is set by tuning the reference frequency generator and verifying resultant frequency offset

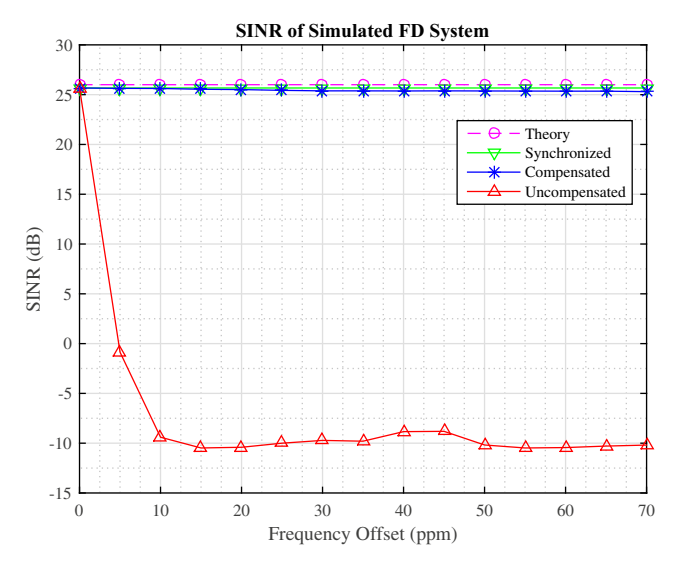


Figure 8 Performance of simulated FD system.

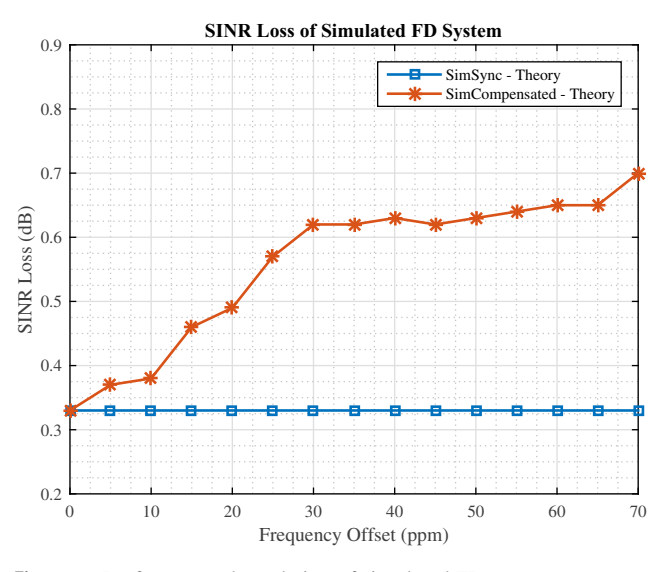


Figure 9 Performance degradation of simulated FD systems.



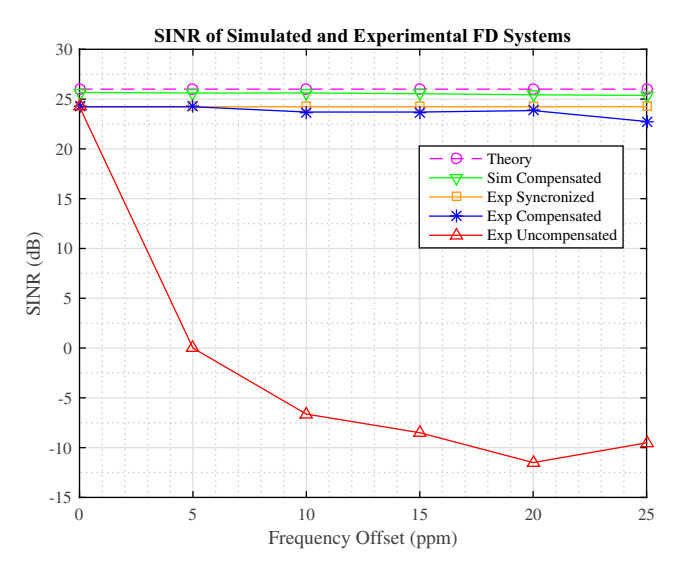


Figure 10 Performances of experimental and simulated FD systems.

amount by the estimation algorithm running at the receiver. Experimental results are presented in Fig. 10. To facilitate comparison, theoretical, simulated and experimental results, are overlapped in Fig. 10.

Figure 11 illustrates the difference between the wired synchronized experimental system and the compensated experimental system. At small offsets, no measurable difference is recorded up to 5 ppm, at which a degradation in the compensated system is measured and gradually increases, but remains within 0.5 dB up to 20 ppm. Between 20 ppm and 25 ppm, there is a sharp increase in SINR loss by 1dB, which is attributed to the measurement equipment reference clock offset operating at its limits.

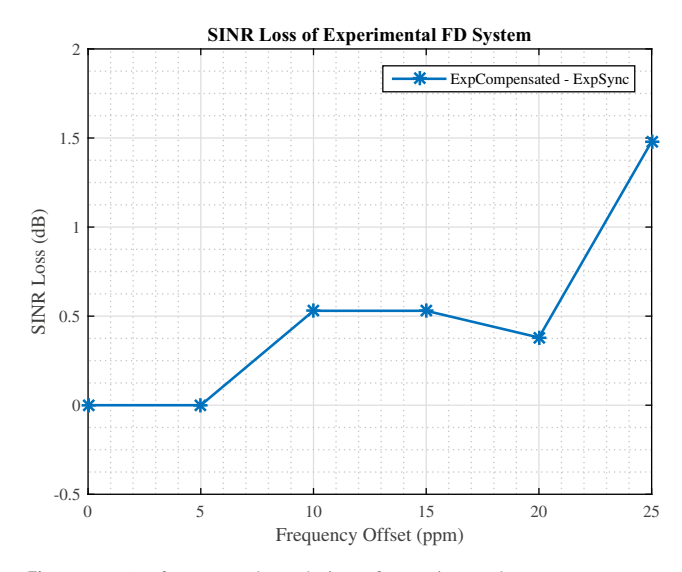


Figure 11 Performance degradation of experimental systems.

### **5 Conclusion**

This paper discussed practical considerations for Full Duplex enabled Integrated Access and Backhaul relay design. Consideration such as passive suppression for FD systems and timing and frequency offset recovery loops are presented. Experimental results showing up to 65 dB of passive suppression and loop recovery with up to 70 ppm of frequency offset are presented.

 $\begin{tabular}{ll} \bf Acknowledgments & The authors gratefully acknowledge support from the National Science Foundation under award number 1710746 \ . \end{tabular}$ 

## References

- Andrews, J.G. (2013). Seven ways that hetnets are a cellular paradigm shift. *IEEE Communications Magazine*, 51(3), 136– 144.
- Anpalagan, A., Bennis, M., Vannithamby, R. (2015). Design and deployment of small cell networks.
- Bennis, M., Simsek, M., Czylwik, A., Saad, W., Valentin, S., Debbah, M. (2013). When cellular meets WiFi in wireless small cell networks. *IEEE Communications Magazine*, 51(6), 44– 50
- Hosseini, K., Hoydis, J., Brink, S., Debbah, M. (2013). Massive MIMO and Small Cells: How to densify heterogeneous networks. Proceedings - IEEE International Conference on Communications (ICC) (pp. 5442–5447).
- Liu, A., & Lau, V. (2014). Hierarchical interference mitigation for massive MIMO cellular networks. *IEEE Transactions on Signal Processing*, 62(18), 4786–4797.
- Hossain, E., Rasti, M., Tabassum, H., Abdelnasser, A. (2014). Evolution toward 5G multi-tier cellular wireless networks: An interference management perspective. *IEEE Wireless Communications*, 21(3), 118–127.
- Bhushan, N., Li, J., Malladi, D., Gilmore, R., Brenner, D., Damnjanovic, A., Sukhavasi, R.T., Patel, C., Geirhofer, S. (2014). Network densification: the dominant theme for wireless evolution into 5G. *IEEE Communications Magazine*, 52(2), 82–89.
- 8. Wei, Z., Zhu, X., Sun, S., Huang, Y., Al-Tahmeesschi, A., Jiang, Y. (2016). Energy-Efficiency of Millimeter-Wave Full-Duplex relaying systems challenges and solutions. *IEEE Access*, 4, 4848–4860.
- 3GPP. NR; Study on integrated access and backhaul; Release 15. 2018
- Sabharwal, A., Schniter, P., Guo, D., Bliss, D.W., Rangarajan, S., Wichman, R. (2014). In-band full-duplex wireless Challenges and opportunities. *IEEE Journal on Selected Areas in Communica*tions, 32(9), 1637–1652.
- Song, L., Wichman, R., Li, Y., Han, Z. (2017). Full-duplex communications and networks.
- Elbamby, M.S., Bennis, M., Saad, W., Debbah, M., Latva-aho, M. (2017). Resource optimization and power allocation in in-band full duplex-enabled non-orthogonal multiple access networks. *IEEE Journal on Selected Areas in Communications*, 35(12), 2860–2873.
- Hong, S., Brand, J., Choi, J.I., Jain, M., Mehlman, J., Katti, S., Levis, P. (2014). Applications of self-interference cancellation in 5G and beyond. *IEEE Communications Magazine*, 52(2), 114– 121.



- Liu, G., Yu, F.R., Member, S., Ji, H., Member, S., Leung, V.C.M., Li, X. (2015). In-Band Full-Duplex Relaying A Survey. Research Issues and Challenges, 17(2), 500–524.
- Zhang, Z., Chai, X., Long, K., Vasilakos, A.V., Hanzo, L. (2015).
   Full duplex techniques for 5G networks: self-interference cancellation, protocol design, and relay selection. *IEEE Communications Magazine*, 53(5), 128–137.
- Du, J., Onaran, E., Chizhik, D., Venkatesan, S., Valenzuela, R.A. (2017). Gbps User Rates Using mmWave Relayed Backhaul With High-Gain Antennas. *IEEE Journal on Selected Areas in Communications*, 35(6), 1363–1372.
- Behbahani, A.S., Merched, R., Eltawil, A.M. (2008). Optimizations of a MIMO relay network. *IEEE Transactions on Signal Processing*, 56(10 II), 5062–5073.
- Sabharwal, A., Schniter, P., Guo, D., Bliss, D.W., Rangarajan, S., Wichman, R. (2013). In-Band Full-Duplex Wireless: Challenges and Opportunities 32(9), 1–22.
- Ahmed, E., Eltawil, A.M., Li, Z., Cetiner, B.A. (2015).
   Full-Duplex Systems using multireconfigurable antennas. *IEEE Transactions on Wireless Communications*, 14(11), 5971–5983.
- Shaboyan, S., Behbahani, A.S., Ahmed, M. (2018). Eltawil active cancellation of Self-Interference for Full-Duplex amplify and forward Wi-Fi relay.
- Shaboyan, S., Ahmed, E., Behbahani, A.S., Younis, W., Eltawil, A.M. (2017). Frequency and Timing Synchronization for In-Band Full-Duplex OFDM System. In GLOBECOM.
- Michele, M., Jay Kuo, C.-C., Pun, M.-O. (2007). Synchronization Techniques for Orthogonal Frequency Division Multiple Access (OFDMA): A tutorial review. *Proceedings of the IEEE*, 95(7), 1394–1427.

**Publisher's Note** Springer Nature remains neutral with regard to jurisdictional claims in published maps and institutional affiliations.



Sergey Shaboyan received the B.Sc. and M.Sc. degrees for the Electrical Engineering Department, University of California Los Angeles, in 2009 and 2011, respectively. He is currently a PhD student at University of California Irvine. His research interest includes full-duplex wireless communications, digital signal processing, hardware and algorithm design for wireless communication systems.



Alireza S. Behbahani received the B.Sc. degree in electrical engineering from Tehran Polytechnic, Tehran, Iran, in 1992, the M.S. degree (with Honors) in electrical engineering from K. N. Toosi University of Technology, Tehran, Iran, in 1996, and the Ph.D. degree in electrical engineering from the University of California, Irvine (UC Irvine), in 2009. He is currently a researcher at the Department of Electrical Engineering and Computer

Science, University of California, Irvine. He is a member of the Center for Pervasive Communications and Computing (CPCC), where he has been a recipient of the UC Irvine CPCC graduate fellowship for the year 2007–2008. His research interests include distributed estimation and detection, machine learning, deep learning, signal processing and its application in wireless communications. Dr. Behbahani has been on the technical program committees and reviewer for several symposia, conferences, and journals in the area of signal processing and wireless communications.



Ahmed M. Eltawil is a Professor at the University of California, Irvine. He has been with the Department of Electrical Engineering and Computer Science since 2005 where he is the founder and director of the Wireless Systems and Circuits Laboratory. His current research interests are in the general area of low power digital circuit and signal processing architectures with an emphasis on mobile computing and communication systems. In addition to

his department affiliation, he is also affiliated to a number of research centers across the University of California, Irvine. He received the Doctorate degree from the University of California, Los Angeles, in 2003 and the M.Sc. and B.Sc. degrees (with honors) from Cairo University, Giza, Egypt, in 1999 and 1997, respectively. Dr. Eltawil has been on the technical program committees and steering committees for numerous workshops, symposia, and conferences in the areas of low power computing and wireless communication system design. He received several awards, as well as distinguished grants, including the NSF CAREER grant supporting his research in low power systems.

